Preprints of the 19th World Congress
The International Federation of Automatic Control
Cape Town, South Africa. August 24-29, 2014

Automatic Retraction Phase of Airborne Wind Energy Systems ⋆

Aldo U. Zgraggen * **Lorenzo Fagiano** ** **Manfred Morari** *

* *Automatic Control Laboratory, ETH Zürich, Switzerland (e-mail: zgraggen|morari@control.ee.ethz.ch).*
** *Corporate Research Center, ABB Schweiz Ltd., Switzerland (e-mail: lorenzo.fagiano@ch.abb.com).*

Abstract: Airborne wind energy systems are an emerging technology to harvest wind energy at higher altitude. Renewable energy is produced by exploiting the aerodynamic lift exerted by a wing tethered to the ground and controlled to fly crosswind paths. System realizations with either on-board or ground-based generation are possible. The focus of this paper is on ground-based generation systems where a two phase cycle is carried out. In the traction phase, power is produced by reeling-out the tether, which is coiled around drums connected to generators; in the retraction phase, the tether is reeled-in after the maximum length has been reached. A new flight controller for the retraction phase, which is straightforward to implement and tune, is proposed and a theoretical analysis and simulation results are presented.

Keywords: Control of renewable energy resources; Control system design.

1. INTRODUCTION

Airborne wind energy (AWE) systems aim to harness wind energy beyond the altitude of traditional wind mills, in stronger and more steady winds, using tethered wings, see Fagiano and Milanese (2012); Diehl et al. (2014) for an overview. Two different system realizations are being studied by several research groups in industry and academia, where the main difference is the placement of the generators. A first theoretical study of the two approaches has been published by Loyd (1980). The first concept considers on-board generators and using an electrified tether to transfer the energy down to the ground, see e.g. Makani Power Inc. (2013), while the second approach exploits the traction force of the tether, which is wound around drums installed on the ground and connected to generators, see e.g. Canale et al. (2010).

In this paper, the second approach is considered where a two-phase cycle, or power cycle, is flown. In the first phase, the traction phase, energy is produced by unreeling the tether from the drums under maximum traction force by flying a crosswind path, i.e. a trajectory roughly perpendicular to the wind. Once the tether has reached its maximum length, the second phase, the retraction phase, starts by recoiling the cable under minimal load and consuming a fraction of the energy previously produced.

The automatic control of tethered wings plays a major role for the operation of this kind of system and has been studied in various publications, see Ilzhöfer et al. (2007); Baayen and Ockels (2012); Williams et al. (2008); Houska and Diehl (2007); Costello et al. (2013); Diehl (2001); Canale et al. (2010). Most of these approaches consider only the problem of flying crosswind figures where the energy is produced. However, for ground-based generation systems also the retraction of the tether has to be done autonomously. In Canale et al. (2010) and Ilzhöfer et al. (2007) a controller for the retraction phase, using a nonlinear Model Predictive Control strategy, has been proposed. These contributions represent interesting applications of advanced control strategies, however their use in a real system appears to be not trivial, due to the discrepancies between the employed simplified model and the real system dynamics of a tethered wing, the need to solve complex nonlinear optimization problems in real-time, and finally the difficulty in tuning the controller in field tests. Indeed, there are very few contributions in the literature, showing experimental results of fully autonomous retraction phases and pumping cycles. In this paper, we contribute to fill this gap by proposing a control scheme for the retraction phase, building on the strategy presented in Fagiano et al. (2013b) for automatic crosswind flight, hence completing the control structure to fly fully autonomous power cycles with a tethered wing with ground-based generation. The proposed controller is easy to implement and tune and, differently from many of the mentioned approaches, does not depend on a measurement of the wind speed at the wing's location, but just a rough estimate of the wind direction. In addition to the control approach, we present a theoretical analysis that highlights its robustness against model mismatch and external disturbances, as well as simulations results.

2. SYSTEM DESCRIPTION

We consider an AWE system with ground-based generation and steering actuation, where a wing is connected with three lines to the ground unit (GU). This setup corresponds to the prototype built at the Fachhochschule Nordwestschweiz as part of the Swiss Kite Power project,

⋆ This research has received partial funding from the Swiss Competence Center Energy and Mobility (CCEM).

Swiss Kite Power (2013b), see Fig. 1. The system has three lines on separated drums connected to the wing. The middle line, called power line, connected to the leading edge of the wing, sustains the main portion of the traction force, while the other two lines, connected to the wing tips, are called steering lines and they are used to influence the wing's trajectory. A shorter left line induces a counter-clockwise turn of the wing as seen from the GU, and vice-versa, hence issuing the required steering deviation. Each drum on the GU is connected to a motor which acts as a generator during traction phase and is used to recoil the tether during the retraction phase. The drum of the power line is connected to a 10 kW motor and each drum of the steering lines to a 5 kW motor, resulting in a rated power of 20 kW. The system is operated with tether lengths up to 200 m. We first recall a dynamical model of the described system and the definition of the velocity angle, which acts as one of the main feedback variables in our approach.

Fig. 1. Lead-out sheaves of the Swiss Kite Power prototype while flying a three line kite.

2.1 Model Equations

We consider a point-mass model already employed in previous work (see e.g. Canale et al. (2010) and references therein) and follow the same notion as presented in Fagiano et al. (2013b). We define an inertial frame $G \doteq (X, Y, Z)$, centered at the GU, with the X axis parallel to the ground, contained in the longitudinal symmetry plane of the GU and pointing downwind, the Z axis pointing upwards, and the Y axis to form a right hand system. The wing's position can be expressed in the inertial frame using spherical coordinates $\varphi(t), \vartheta(t), r(t)$ as (see Fig. 2):

$$ {}_G\mathbf{p}(t) = \begin{pmatrix} r(t)\cos(\varphi(t))\cos(\vartheta(t)) \\ r(t)\sin(\varphi(t))\cos(\vartheta(t)) \\ r(t)\sin(\vartheta(t)) \end{pmatrix}, \qquad (1) $$

where t is the continuous time variable. In (1) and throughout the paper, vectors are denoted as bold variables and the subscript letter in front of vectors (e.g. ${}_G\mathbf{p}(t)$) denotes the reference system considered to express the vector components. Additionally, we denote unit vectors by $\mathbf{e}$ followed by a subscript indicating the related axis, e.g. $\mathbf{e}_x$ denotes the unit vector of the X axis in the inertial frame G.

If the tether length r is kept constant, the wing cannot fly upwind, surpassing its anchor point against the wind.

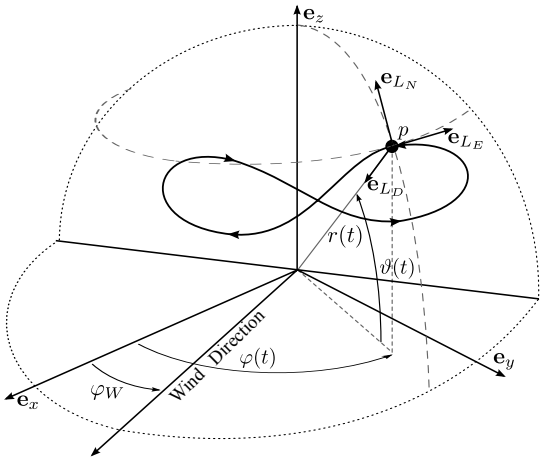

Fig. 2. The wing's position p (black dot) is shown on a figure eight path together with the local coordinate frame L.

Thus, its motion is restricted on a quarter sphere defined by the tether length r, the ground plane $(\mathbf{e}_x, \mathbf{e}_y)$, and a vertical plane perpendicular to the wind direction and containing the anchor point of the tether (see Fig. 2, dotted lines). This quarter sphere is called "wind window". We define also a non-inertial coordinate system $L \doteq (L_N, L_E, L_D)$, centered at the wing's position (depicted in Fig. 2). The L_N axis, or local north, is tangent to the sphere of radius r, on which the wing's trajectory evolves, and points towards its zenith. The L_D axis, called local down, points to the center of the sphere (i.e. the GU), hence is perpendicular to the tangent plane of the sphere at the wing's location. The L_E axis, named local east, forms a right hand system and spans the tangent plane together with L_N. The system L is a function of the wing's position only. The transformation matrix to express vectors in the local frame L from the inertial frame G is:

$$ A_{LG} = \begin{pmatrix} -\sin(\vartheta)\cos(\varphi) & -\sin(\vartheta)\sin(\varphi) & \cos(\vartheta) \\ -\sin(\varphi) & \cos(\varphi) & 0 \\ -\cos(\vartheta)\cos(\varphi) & -\cos(\vartheta)\sin(\varphi) & -\sin(\vartheta) \end{pmatrix} \qquad (2) $$

The dynamic equations of the model are derived from first principles and the wing is assumed to be a point with given mass. The tether is assumed to be straight with a non-zero diameter. The aerodynamic drag of the tether and the tether mass are added to the wing's drag and mass, respectively. The effects of gravity and inertial forces are also considered. The wing is assumed to be steered by a change of the roll angle ψ, which is manipulated by the control system via the line length difference δ. By applying Newton's law of motion to the wing in the reference system L we obtain:

$$ \left| \begin{aligned} \ddot{\vartheta} &= \tfrac{\mathbf{F}\cdot\mathbf{e}_{L_N}}{rm} - \sin(\vartheta)\cos(\vartheta)\dot{\varphi}^2 - \tfrac{2}{r}\dot{\vartheta}\dot{r} \\ \ddot{\varphi} &= \tfrac{\mathbf{F}\cdot\mathbf{e}_{L_E}}{rm\cos(\vartheta)} + 2\tan(\vartheta)\dot{\vartheta}\dot{\varphi} - \tfrac{2}{r}\dot{\varphi}\dot{r} \\ \ddot{r} &= -\tfrac{\mathbf{F}\cdot\mathbf{e}_{L_D}}{m} + r\dot{\vartheta}^2 + r\cos^2(\vartheta)\dot{\varphi}^2 \end{aligned} \right| , \qquad (3) $$

where m is the mass of the wing. The force $\mathbf{F}(t)$ consist of contributions from gravity and aerodynamic forces, see Fagiano et al. (2013b) for details. Note that for simplicity of notation we dropped the time dependence of the involved parameters in (2) and (3).

In a recent contribution concerned with the autonomous flight along figure eight paths during traction phase, the notion of the velocity angle γ has been introduced (see Fagiano et al. (2013b)), defined as:

$$\gamma(t) \doteq \arctan\left(\frac{\mathbf{v}_P(t)\cdot\mathbf{e}_{L_E}(t)}{\mathbf{v}_P(t)\cdot\mathbf{e}_{L_N}(t)}\right) \tag{4}$$

$$= \arctan\left(\frac{\cos\vartheta(t)\,\dot{\varphi}(t)}{\dot{\vartheta}(t)}\right). \tag{5}$$

Thus, the angle $\gamma(t)$ is the angle between the local north $\mathbf{e}_{L_N}(t)$ and the projection of the wing's velocity vector $\mathbf{v}_P(t)$ onto the tangent plane of the wind window. In (5) the four-quadrant version of the arc tangent function shall be used, such that $\gamma(t)\in[-\pi,\pi]$. The velocity of the wing with respect to the GU in the L frame is defined as

$${}_L\mathbf{v}_P(t) = \begin{pmatrix} r(t)\dot{\vartheta}(t) \\ r\cos\vartheta(t)\,\dot{\varphi}(t) \\ -\dot{r}(t)\end{pmatrix}. \tag{6}$$

The velocity angle is particularly suited as a feedback variable since it describes the flight conditions of the wing with just one scalar: as an example, if $\gamma=0$ the wing is moving upwards towards the zenith of the wind window, if $\gamma=\pi/2$ the wing is moving parallel to the ground towards the local east, finally if $\gamma=\pi$ the wing is flying towards the ground. We note that $\gamma(t)$ is in general different from the heading angle of the wing. Additionally, a control-oriented model for tethered wings, originally proposed by Erhard and Strauch (2013) and refined in Fagiano et al. (2013b), has been used for the control design:

$$\dot{\gamma}(t) \simeq K(t)\delta(t) + T(t)\,, \tag{7}$$

where

$$K(t) = \frac{\rho C_L(t) A|\mathbf{v}(t)|}{2md_s}\left(1+\frac{1}{E_{eq}^2}\right)^2 \tag{8a}$$

$$T(t) = \frac{g\cos\vartheta(t)\,\sin\gamma(t)}{|\mathbf{v}(t)|} + \sin\vartheta(t)\,\dot{\varphi}(t)\,. \tag{8b}$$

In (7) and (8) the steering input, i.e. line length difference of the steering lines, is denoted by $\delta(t)$, ρ is the air density, $C_L(t)$ is the aerodynamic lift coefficient, A is the reference area of the wing, d_s is the span of the wing, E_{eq} is the equivalent efficiency of the wing $E_{eq}\doteq C_L(t)/C_{D,eq}(t)$ where $C_{D,eq}(t)$ represents the drag coefficient of the wing and lines together, and g is the gravity acceleration. In (8), the apparent wind speed is denoted by $\mathbf{v}(t)$, defined as

$$\mathbf{v}(t) = \mathbf{v}_W(t) - \mathbf{v}_P(t)\,, \tag{9}$$

where $\mathbf{v}_W(t)$ is the wind velocity vector.

The model (7) has been validated through experimental data with good correspondence in a wide range of operating conditions, see Fagiano et al. (2013b). We show next that this model can, with some modifications, be used to describe the wing's steering dynamics also during the retraction phase. The main difference between the two phases is that during retraction the wing's speed in the tangent plane $\mathbf{v}_P^p(t)$ to the wind window is close to zero, thus making a modification of the definition of the velocity angle (5) necessary. As it can be seen from (7), the steering behavior of the wing depends on the apparent wind speed, which is dominated by $\mathbf{v}_P(t)$ during crosswind flight in the traction phase. However, during the retraction phase a small traction force is desired which can be achieved by flying the wing to the border of the wind window, where $\mathbf{v}_P(t)$ is low and mainly consist of the reel-in speed $\dot{r}$. Thus, the apparent wind speed will be determined by the wind speed $\mathbf{v}_W$ and the reel-in speed $\dot{r}$. From (7), it can be seen that as long as the gain $K(t)$ is different from zero, i.e. either $\mathbf{v}_W$ or $\dot{r}$ are non-zero, the steering gain $K(t)$ is positive and it is possible to steer the wing. In section 3, we will show that indeed it is possible to stabilize the wing as long as $K(t)>0$.

2.2 Regularized Velocity Angle

We will now define a modified version of the velocity angle (5) such that it can be used as feedback variable for the retraction phase of a ground-based generation AWE system, when $\mathbf{v}_P^p$ is close to zero. During retraction, the tethers have to be recoiled onto the drums under minimal traction force such that only a small fraction of the previously generated power is used. To achieve this goal with no pitch control, the wing has to be flown at the border of the wind window, in a static angular position w.r.t. GU. In these conditions, the velocity angle γ as computed in (5) becomes undefined, so that this variable can not be used for feedback control anymore.

Since the wing stays in a static position in terms of φ and ϑ, the apparent wind speed corresponds to the wind speed $\mathbf{v}_W(t)$ at the wing's position plus the reel-in speed $\dot{r}(t)$. For simplicity, we assume that the wind flow is parallel to the ground, i.e. the $(\mathbf{e}_x,\mathbf{e}_y)$ plane, and its direction is at an angle φ_W w.r.t to $\mathbf{e}_x$ (see Fig. 2). It is also assumed that the wing is designed so that it orientates itself into the wind, i.e. its longitudinal symmetry axis is aligned with the wind direction. This effect can be achieved by a wing equipped with a rudder or a curved shape, like C-shaped surf kites. Thus, the apparent velocity of the wing in the tangent plane to the wind window is equal to the wind velocity projected in the same plane. The wind vector in the inertial frame, ${}_G\mathbf{v}_W$, can be written as (recalling the assumption that the wind is parallel to the ground)

$${}_G\mathbf{v}_W = \begin{pmatrix} W_0\cos(\varphi_W) \\ W_0\sin(\varphi_W) \\ 0\end{pmatrix}, \tag{10}$$

where W_0 stands for the wind speed. Using A_{LG} in (2), the wind vector in the L frame is given as

$${}_L\mathbf{v}_W = \begin{pmatrix} -W_0\sin\vartheta\cos(\varphi-\varphi_W) \\ -W_0\sin(\varphi-\varphi_W) \\ -W_0\cos\vartheta\cos(\varphi-\varphi_W)\end{pmatrix}. \tag{11}$$

Since the wing is assumed to be aligned with the wind direction, we can define its orientation $\beta(t)$ w.r.t to the local north, similarly to (4)-(5), as

$$\beta(t) \doteq \arctan\left(\frac{-{}_L\mathbf{v}_W(t)\cdot\mathbf{e}_{L_E}(t)}{-{}_L\mathbf{v}_W(t)\cdot\mathbf{e}_{L_N}(t)}\right) \tag{12}$$

$$= \arctan\left(\frac{\sin(\varphi-\varphi_W)}{\sin\vartheta\cos(\varphi-\varphi_W)}\right), \tag{13}$$

which is the angle between $\mathbf{e}_{L_N}$ and the longitudinal symmetry axis of the wing. Note that for notational simplicity we dropped the time dependence of the variables in (13). From (13), assuming without loss of generality $\varphi_W=0$, we can see that $\beta(t)$ converges to $\pm\pi/2$ if the wing approaches the border of the wind window, e.g $\varphi(t)\approx\pm\pi/2$. An estimate of the wind direction φ_W can be either obtained by measurements provided by ground

based sensors or by processing the measurements of the line force collected during the traction phase, see e.g. Zgraggen et al. (2013).

The considerations presented so far lead to the idea of extending the definition of the velocity angle γ by a regularization term such that the wing's orientation is also defined for static positions of the wing. In particular, we define the regularized velocity angle as

$$\gamma^r = \arctan\left(\frac{\cos(\vartheta)\dot{\varphi} + c\sin(\varphi - \varphi_W)}{\dot{\vartheta} + c\sin\vartheta\cos(\varphi - \varphi_W)}\right), \qquad (14)$$

where $c > 0$ is a scalar chosen by the control designer. In principle, the value of c should reflect the magnitude of the absolute wind speed, which might be quite difficult to obtain. However, in our simulations and experiments the system behavior resulted to be not sensitive to this quantity. Thus, according to (14) during the traction phase when the speed of the wing is significantly larger than the wind speed we have $\gamma^r(t) \approx \gamma(t)$, but during the retraction phase, when the wing speed approaches zero, $\gamma^r(t)$ still provides a reasonable value whereas $\gamma(t)$ of (5) becomes undefined. A comparison between $\gamma(t)$ and $\gamma^r(t)$ during a flight test is shown in Fig. 3.

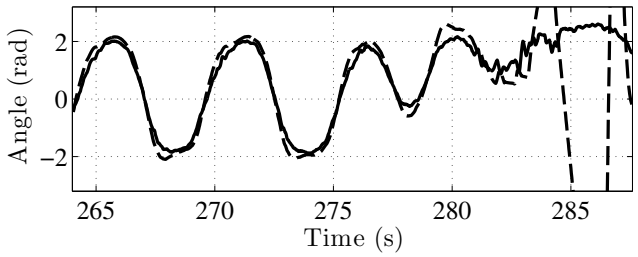

Fig. 3. Experimental data. Time courses of $\gamma(t)$ (dashed) and $\gamma^r(t)$ (solid) during a transition from flying figure-eight paths in crosswind conditions (up to approximately 282 s) to a position at the border of the wind window.

With the regularized velocity angle (14) we can now adopt a similar control scheme for the retraction phase as the one used for the traction phase controller described in Fagiano et al. (2013b), which will be discussed in the next section.

3. RETRACTION CONTROL SCHEME

We consider a hierarchical control scheme as proposed in Fagiano et al. (2013b), consisting of three nested loops, shown in Fig. 4. Note that some feedback variables, in particular the regularized velocity angle, cannot be directly measured and need to be estimated, see Fagiano et al. (2013a) for details. The main difference between the re-

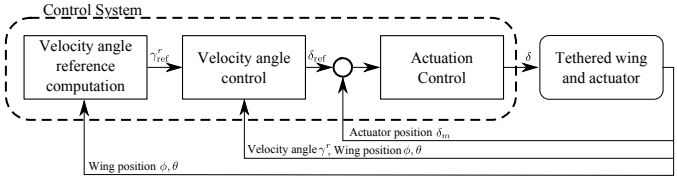

Fig. 4. Control scheme overview

traction phase and the traction phase lies in the computation of the velocity angle reference γ^r_{ref}, and instead of the velocity angle γ we use the regularized velocity angle γ^r as feedback variable. Therefore, we will only recall briefly the equations describing the inner control loops for the sake of completeness (see Fagiano et al. (2013b)) and focus here on the outer control loop, responsible for providing the velocity angle controller with a suitable reference.

Neglecting higher-order effects and external disturbances, the actuation system can be modeled as a second order system. The closed loop system for the actuation control loop is then given by

$$\ddot{\delta}_m = \omega_{\text{cl}}^2\delta_{\text{ref}} - 2\zeta_{\text{cl}}\omega_{\text{cl}}\dot{\delta}_m - \omega_{\text{cl}}^2\delta_m\,, \qquad (15)$$

where δ_m is the actuator's position, δ_{ref} is the actuator's position reference, and ω_{cl} and ζ_{cl} are the natural frequency and damping, respectively, of the actuation control loop. The manipulated variable is $\delta = K_\delta\delta_m$, where K_δ is a known constant depending on the mechanical setup of the system. In our case, $K_\delta = 1$. The velocity angle control loop consists of a proportional controller given by

$$\delta_{\text{ref}} = K_c\left(\gamma^r_{\text{ref}} - \gamma^r\right)\,, \qquad (16)$$

where the gain K_c is chosen by the designer. More details about the inner loops can be found in Fagiano et al. (2013b).

In order to minimize the line force, the goal of the retraction controller is to stabilize the wing at a static position in terms of φ and ϑ at the border of the wind window, e.g. $\varphi - \varphi_W = \pm\pi/2$, and at a given elevation angle ϑ_{ref}. As seen in the previous section from (14), we have $\gamma^r = \pi/2$ for a static position of the wing with $\varphi - \varphi_W = \pi/2$. This corresponds to a wing position on the left of the wind window as seen from the GU. Similarly, if a position on the right of the wind window is considered, i.e. $\varphi - \varphi_W = -\pi/2$, the regularized velocity angle becomes $\gamma^r = -\pi/2$. For simplicity, we will now only consider positions on the left of the wind window for the retraction phase, i.e. $\varphi - \varphi_W = \pi/2$. However, the approach can be directly applied also for positions on the right side of the wind window.

Using the point-mass model of the tethered wing, it can be shown that there exist equilibrium points at the border of the wind window, whose values are a function (for a given wing) of the steering input δ and the absolute wind speed. These equilibrium points can be found as usual by setting all time derivatives of the model states to zero and solving (3) for a given steering input. Additionally, they can also be found by numerical simulations of the point-mass model employing a constant steering input. This suggest that these equilibrium points are indeed stable and have a non-empty region of attraction, as it is revealed also by commonly used analysis techniques (see e.g. Khalil (2001)).

Inspired by the above considerations, we propose the following feedback control strategy to compute a reference value for the velocity angle:

$$\gamma^r_{\text{ref}} = K_\vartheta(\vartheta_{\text{ref}} - \vartheta) + \frac{\pi}{2}, \qquad K_\vartheta < 0\,, \qquad (17)$$

where ϑ_{ref} is a reference elevation angle chosen by the user, which should theoretically correspond to an equilibrium point for the wing at the side of the wind window. From (17), one can note that, if the elevation of the wing is smaller than the reference elevation, the velocity angle

reference is smaller than $\pi/2$, thus demanding the wing to move towards the zenith of the wind window, and vice-versa for a larger elevation than the reference elevation we have $\gamma^r_{\text{ref}} > \pi/2$. This reference is saturated to $\gamma^r_{\text{ref}} \in [\gamma_{\min}, \gamma_{\max}]$ to prevent the wing from doing fast maneuvers which would increase the traction force unnecessarily.

The scalar gain K_c for the velocity angle controller and the scalar gain K_ϑ for the velocity angle reference computation are chosen by the designer. By using (17) in the outer loop of the control scheme (see Fig. 4), the resulting control system is linear (time varying) and controller gains K_ϑ and K_c can be found, such that robust stability is achieved in the face of model uncertainty and different wind conditions. In particular, we can rewrite the system dynamics given by (7), (15)-(17) in terms of angle errors $\Delta\vartheta, \Delta\gamma^r$ and the position and velocity of the actuation system δ_m and $\dot{\delta}_m$. In order to formulate these error dynamics we need an intermediate step to include the dynamics of the angle ϑ. To this end, we note that the apparent wind velocity component in the tangent plane, $|\mathbf{v}^p|$, in ϑ direction, given by $r\dot{\vartheta}$, is by definition of γ equal to $|\mathbf{v}^p|\cos\gamma$ (compare (5)). Since the wing tends to align itself with the wind direction, we assume that $\pi/2 - \gamma^r$ is small, so that we can linearize its trigonometric functions. Then, the dynamics of the ϑ angle can, after some manipulations, be written as:

$$\dot{\vartheta} = \frac{|\mathbf{v}^p|}{r}\left(\frac{\pi}{2} - \gamma^r\right). \tag{18}$$

Since the nominal value for the velocity angle reference is γ^r_{ref} and the targeted ϑ angle of the wing is ϑ_{ref}, the tracking errors for these two variables are defined as:

$$\Delta\gamma^r = \gamma^r_{\text{ref}} - \gamma^r \tag{19}$$
$$\Delta\vartheta = \vartheta_{\text{ref}} - \vartheta\,. \tag{20}$$

We can now state the system dynamics given by (7),(15)-(18), and $\mathbf{x} = [\Delta\vartheta, \Delta\gamma^r, \delta_m, \dot{\delta}_m]^T$ (where ^{T} stands for the matrix transpose operation) as

$$\dot{\mathbf{x}} = \underbrace{\begin{bmatrix} K_\vartheta\frac{|\mathbf{v}^p|}{r} & -\frac{|\mathbf{v}^p|}{r} & 0 & 0 \\ K_\vartheta^2\frac{|\mathbf{v}^p|}{r} & -K_\vartheta\frac{|\mathbf{v}^p|}{r} & -KK_\delta & 0 \\ 0 & 0 & 0 & 1 \\ 0 & K_c\omega_{\text{cl}}^2 & -\omega_{\text{cl}}^2 & -2\zeta_{\text{cl}}\omega_{\text{cl}} \end{bmatrix}}_{A_{\text{cl}}} \mathbf{x} + w\,. \tag{21}$$

In (21), the term K corresponds to the uncertain gain in (8a) and depends on the system's parameters as well as the wind and the flight conditions. The term $w \in \mathbb{R}^4$ accounts for effects of gravity and apparent forces of (8b), as well as for the forces exerted by the lines on the actuator. System (21) has time-varying, uncertain linear dynamics characterized by the matrix $A_{\text{cl}}(\Theta)$, where $\Theta = [K, |\mathbf{v}|]$. However, upper and lower bounds for all of the involved parameters can easily be derived on the basis of the available knowledge on the system. These bounds can be employed to compute points Θ^i, $i = 1, \ldots, n_v$, such that $\Theta \in \text{conv}(\Theta^i)$, where conv denotes the convex hull. Then, the closed-loop system (21) results to be robustly stable if there exists a positive definite matrix $P = P^T \in \mathbb{R}^{4x4}$ such that (see e.g. Amato (2006)):

$$A_{\text{cl}}^T(\Theta^i)P + PA_{\text{cl}}(\Theta^i) \prec 0,\ i = 1, \ldots, n_v\,, \tag{22}$$

Condition (22) can be easily checked by using an LMI solver. In section 4 we show with simulations and experiments that indeed a single pair (K_c, K_ϑ) achieves robust stability of the control system, as predicted by the described theoretical analysis. The two scalar gains, i.e. the values of K_c and K_ϑ, can be tuned at first by using the equations (7) and (17), and then via experiments.

Table 1. System Parameters

Name	Symbol	Value	Unit
Wing effective area	A	9	m^2
Kite span	d_s	3.5	m
Kite mass	m	2.45	kg
Tether length	r	$[50 \ldots 150]$	m
Tether diameter	d_t	0.003	m
Tether density	ρ_t	970	kg/m^3
Air density	ρ	1.2	kg/m^3

Table 2. Control Parameters

Name	Symbol	Value	Unit
Control loop damping	ζ_{cl}	0.7	
Control loop natural frequency	ω_{cl}	78	rad/s
Mechanical actuation ratio	K_δ	1	
γ^r feedback gain (traction)	K_c	0.056	
γ^r feedback gain (retraction)	K_c	0.28	
γ^r_{ref} feedback gain (retraction)	K_ϑ	2.5	
Elevation reference (retraction)	ϑ_{ref}	1	rad

4. RESULTS

We tested the proposed approach in simulation, employing the non-linear point-mass model for tethered wings (3). The main system's parameters and controller's parameters are shown in Tables 1 and 2, respectively. The values of the gains in the Table 2 indeed satisfy condition (22) for a wide range of operating conditions. In Fig. 5, the trajectory of the wing from launch until the end of the first power cycle is shown. At first, the wing is flown in crosswind conditions, flying figure-eight paths until it reaches the maximum tether length of 150 m, using the controller described in Fagiano et al. (2013b). Then, the retraction phase is started using the proposed velocity angle reference computation (17) and the tether is reeled-in until a length of 50 m is reached. At that point, the velocity angle reference is switched back to the one proposed in Fagiano et al. (2013b) to complete the power cycle. In Fig. 6, the corresponding time courses of the position angles φ and ϑ during the power cycle are shown. Around 68 s, the controller switches from traction to retraction and stabilizes the wing at $\vartheta_{\text{ref}} = 1$. Note that φ becomes larger than $\pi/2$ due to the reel-in speed and thus surpasses the GU against the wind, compare Fig. 5. Around 147 s, the controller switches from retraction to traction and the wing starts again flying figure-eight paths in crosswind conditions. The time course of the velocity angle and its reference can be seen in Fig. 7.

At present, experimental tests with the described approach have been successfully run. A movie showing autonomous power cycles carried out with the presented technique is available online: Swiss Kite Power (2013a).

5. CONCLUSION

We proposed an approach to design a feedback controller for the retraction phase of an AWE system with ground-

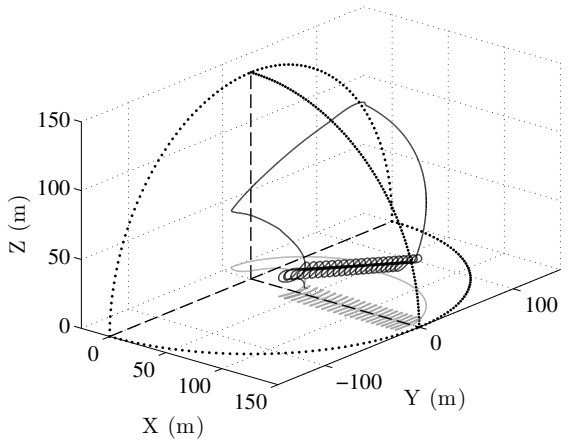

Fig. 5. Simulation results. 3D trajectory (black) of the tethered wing during one flown power cycle and its projection (gray) on the ground.

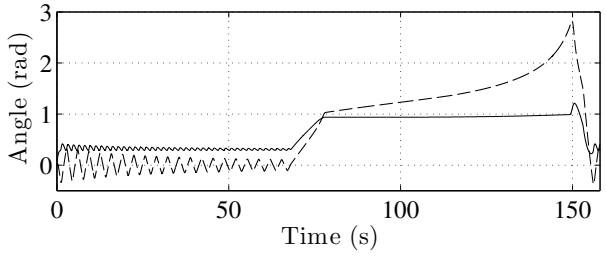

Fig. 6. Simulation results. Time courses of φ (dashed) and ϑ (solid) of one power cycle.

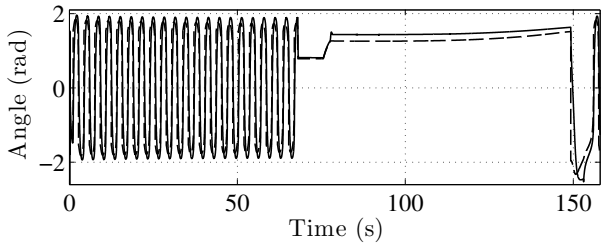

Fig. 7. Simulation results. Time courses of γ^r (solid) and its reference γ^r_{ref} (dashed) during one power cycle.

based generation, where the tether is recoiled onto the drums. Together with the traction controller in Fagiano et al. (2013b) the approach presented here can be used to achieve fully autonomous power cycles. The controller is based on a hierarchical structure and is able to stabilize the wing in a position at the border of the wind window to minimize the traction force. Few parameters, that can be easily tuned, are involved in the design. The approach does not depend on the tether length or reeling speed and thus the latter can still be optimized to maximize the energy output of the system.

ACKNOWLEDGEMENTS

The authors acknowledge the SpeedGoat®'s Greengoat program.

REFERENCES

Amato, F. (2006). *Robust Control of Linear Systems Subject to Uncertain Time-Varying Parameters*, volume 325 of *Lecture Notes in Control and Information Sciences*. Springer Berlin Heidelberg.

Baayen, J.H. and Ockels, W.J. (2012). Tracking control with adaption of kites. *IET Control Theory and Applications*, 6(2), 182–191.

Canale, M., Fagiano, L., and Milanese, M. (2010). High altitude wind energy generation using controlled power kites. *IEEE Transactions on Control Systems Technology*, 18(2), 279 –293.

Costello, S., Franois, G., and Bonvin, D. (2013). Real-time optimization for kites. In *Proceedings of the IFAC Workshop on Periodic Control Systems, Caen, France, 3.-5. July*, 64–69.

Diehl, M. (2001). *Real-Time Optimization for Large Scale Processes*. Ph.D. thesis, Ruprecht-Karls-Universität Heidelberg.

Diehl, M., Schmehl, R., and Ahrens, U. (eds.) (2014). *Airborne Wind Energy*. Green Energy and Technology. Springer Berlin Heidelberg.

Erhard, M. and Strauch, H. (2013). Control of towing kites for seagoing vessels. *Control Systems Technology, IEEE Transactions on*, 21(5), 1629–1640.

Fagiano, L., Huynh, K., Bamieh, B., and Khammash, M. (2013a). On sensor fusion for airborne wind energy systems. *IEEE Transactions on Control Systems Technology*. In press, online version available.

Fagiano, L. and Milanese, M. (2012). Airborne wind energy: an overview. In *American Control Conference 2012*, 3132–3143. Montreal, Canada.

Fagiano, L., Zgraggen, A.U., Morari, M., and Khammash, M. (2013b). Automatic crosswind flight of tethered wings for airborne wind energy: modeling, control design and experimental results. *IEEE Transactions on Control Systems Technology*. In press, online version available.

Houska, B. and Diehl, M. (2007). Optimal control for power generating kites. In *European Control Conference (ECC), Kos, Greece, 2.-5. July*.

Ilzhöfer, A., Houska, B., and Diehl, M. (2007). Nonlinear MPC of kites under varying wind conditions for a new class of large-scale wind power generators. *Int. Journal of Robust and Nonlinear Control*, 17, 1590–1599.

Khalil, H.K. (2001). *Nonlinear Systems*. Prentice Hall, 3 edition.

Loyd, M.L. (1980). Crosswind kite power. *Journal of Energy*, 4(3), 106–111.

Makani Power Inc. (2013). Alameda, CA, USA [Online]. Available: http://www.makanipower.com/.

Swiss Kite Power (2013a). Experimental test movie . Available on–line: `http://youtu.be/yDRc3Ze4GAM`.

Swiss Kite Power (2013b). Windisch, Switzerland [Online]. Available: http://www.swisskitepower.ch/.

Williams, P., Lansdorp, B., and Ockels, W. (2008). Optimal crosswind towing and power generation with tethered kites. *Journal of guidance, control, and dynamics*, 31(1), 81–93.

Zgraggen, A., Fagiano, L., and Morari, M. (2013). On real-time optimization of airborne wind energy generators. In *Conference on Decision and Control*, 385–390. Florence, Italy.